ELSEVIER

Physica B 249–251 (1998) 191–196

PHYSICA B

Coulomb oscillations in few-electron quantum dot

L.P. Kouwenhoven[a,*], T.H. Oosterkamp[a], S. Tarucha[b], D.G. Austing[b], T. Honda[b]

[a] *Department of Applied Physics and DIMES, Delft University of Technology, P.O. Box 5046, 2600 GA Delft, The Netherlands*
[b] *NTT Basic Research Laboratories, 3-1, Morinosoto Wakamiya, Atsugi-shi, Kanagawa 243-01, Japan*

Abstract

We study atomic-like properties of artificial atoms by measuring Coulomb oscillations in vertical quantum dots containing a tunable number of electrons starting from zero. At zero magnetic field the energy needed to add electrons to a dot reveals a shell structure for a two-dimensional harmonic potential. As a function of magnetic field the current peaks shift in pairs, due to the filling of electrons into spin-degenerate single-particle states. When the magnetic field is sufficiently small, however, the pairing is modified, as predicted by Hund's rule, to favour the filling of parallel spins.

Keywords: Quantum dots; Mesoscopic systems

Coulomb oscillations are usually periodic. However, in a small dot containing just a few electrons, both the electron–electron interactions and quantum confinement effects become sufficiently strong that the spacings between the Coulomb oscillation peaks become irregular [1–5]. Lateral dot structures, induced through gates in a 2DEG, are not suitable for defining a system of only a few electrons because the tunnel barriers are formed by a depletion potential. This potential is significantly affected by the center or plunger gate potential close to 'pinch-off'. In practice, when $N < \sim 25$ the tunnel barriers become too large for observing a current, even at resonance. In vertical dot structures, this problem is overcome by the use of heterostructure barriers. These tunnel barriers are abrupt and thin, and are only weakly affected by a gate potential. Furthermore, the lateral geometry in a vertical dot is sufficiently well defined to allow for the formation of systematically degenerate sets of 0D-states in the dot [5]. However, there are inherent technical difficulties in squeezing the vertical dot, i.e. varying the number of electrons. To date there only have been a few reports of how these difficulties have been solved. These include transport through two-terminal dots [6–11], transport through three-terminal gated dots [4,5,12–16], and capacitance measurements on two-terminal gated dots [1].

Fig. 1 shows a schematic diagram of a vertical dot and the Coulomb oscillations observed at $B = 0$ T [5]. This dot has a circular Schottky gate placed on the side of the mesa close to the dot region, and is used to squeeze the dot. The dot is

*Corresponding author. Tel.: 31-15-2786094; fax: 31-15-2783251; e-mail: leo@qt.tn.tudelft.nl.

0921-4526/98/$19.00
PII: S0921-4526(98)00096-9

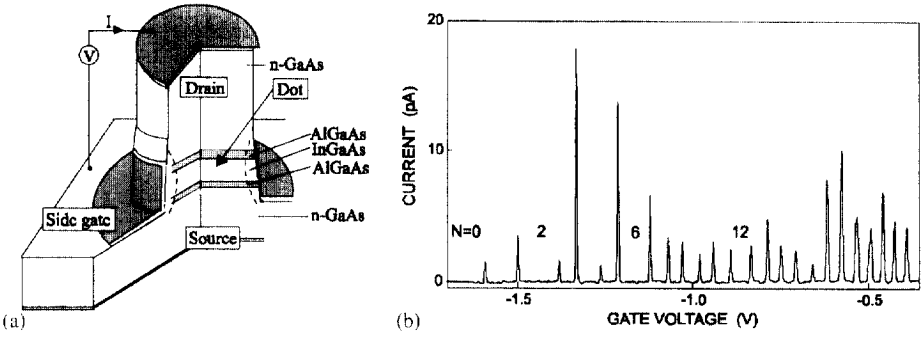

Fig. 1. (a) Schematic diagram of the gated quantum dot device and (b) the Coulomb oscillations in the current versus gate voltage at $B = 0$ T observed for a 0.5 μm diameter dot.

made from InGaAs, which has a narrower band gap than the GaAs in the contacts. The inclusion of In reduces the conduction band bottom in the dot below the Fermi level in the contacts. This means that electrons are accumulated in the dot even when no voltages are applied. This allows to study linear transport properties. The current I versus gate voltage V_g measured at small V_{sd} shows clear Coulomb oscillations.

In Fig. 2 the measured size of the Coulomb gap (i.e. the source–drain voltage at which current starts to flow) is plotted as a function of gate voltage. The vertical $V_{sd} = 0$ axis corresponds directly to the data in Fig. 1b. Note that, for instance, the size of the peak spacings along the $V_{sd} = 0$ axis are the same as the peak spacings for the corresponding N in Fig. 1b. These irregular peak spacings at $V_{sd} = 0$ lead to correspondingly irregular sizes for the diamond shaped Coulomb gaps. As we discuss below these irregularities can be described to the small number of electrons in vertical dots. Note that the Coulomb diamond in the $N = 0$ region never closes when we continue to make the gate voltage more negative, implying that the dot is indeed empty. From this observation the absolute values of N can be identified and used to label the spaces between the current peaks.

If a dot has the shape of a circular disk and the confining potential is harmonic, then we have a system with a high degree of symmetry. This symmetry leads to sets of degenerate single-particle states which form a *shell structure*. Such a shell structure for circular 2D potentials was predicted by self-

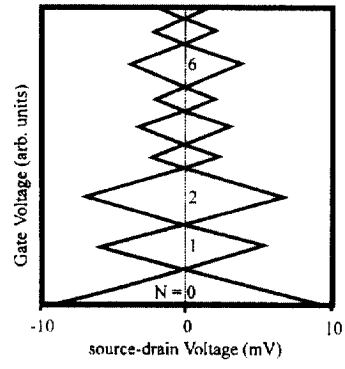

Fig. 2. Measured size of the Coulomb gap versus gate voltage. The diamonds represent the source–drain voltage value at which current starts to flow. The sizes of the diamonds directly correspond to the peak spacings in Fig. 1b.

consistent calculations [17]. Here, we discuss the formation and electron filling of a shell structure by comparing a non-interacting model with models that include Coulomb interactions and exchange interactions.

Fig. 3a shows a comparison between energies of non-interacting single-particle states, classical charging energies derived from a self-capacitance model, and those derived from a Hartree–Fock (HF) calculation. The results are shown in the form of addition energies with respect to N [18]. For a circularly symmetric 2D confinement potential the quantum numbers for the single-particle states are conveniently described by a radial quantum number $n = 0, 1, 2, \ldots$ and an angular momentum

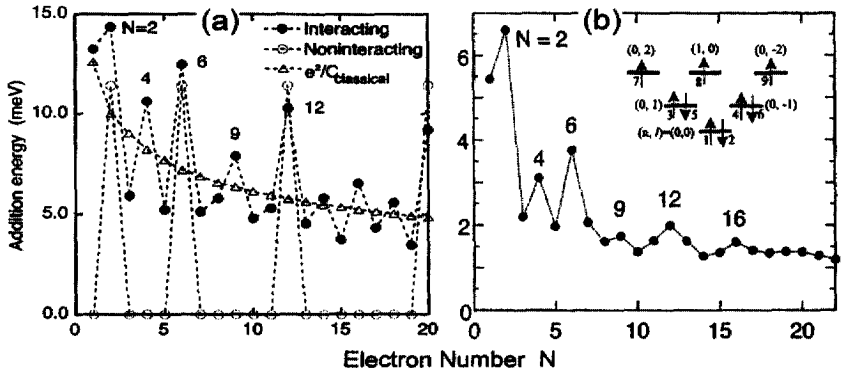

Fig. 3. Addition energy versus electron number. (a) Hartree–Fock calculation for a circular dot with harmonic lateral potential (filled circles). The open circles show the single-particle excitation energy, and the open triangles give the charging energy from a classical self-capacitance model (from Ref. [18]). (b) The filled circles are the measured addition energies derived from the Coulomb oscillations in Fig. 1. The inset depicts the filling of the shells for $N = 9$ in line with Hund's rule.

quantum number $\ell = 0, \pm 1, \pm 2, \ldots$. We consider a harmonic confinement potential $V(r) = \frac{1}{2}m^*\omega_0^2 r^2$ for which the non-interacting Schrödinger equation has the following analytic solutions for the eigenenergies $E_{n\ell}$:

$$E_{n\ell} = (2n + |\ell| + 1)\hbar\omega_0. \quad (1)$$

The calculation in Fig. 3a is performed by taking $\hbar\omega_0 = 2\,Ry^*$ (= 11.5 meV for the InGaAs dot in Fig. 1), where Ry^* is the effective Rydberg constant which is a measure of the interaction energy. It follows from Eq. (1) that $E_{n\ell}$ has degenerate sets of states, which are separated by $\hbar\omega_0$ from each other and which are completely filled for $N = 2, 6, 12, 20$, etc. For these special values of N the addition energy is maximal. These maxima persist when interactions are included in a HF approximation. However, in addition, the HF calculation also reveals maxima in the addition energy at $N = 4$, 9 and 16. For these N values, respectively, the second, third and fourth shells are half filled with parallel spins in accordance with *Hund's rule*. Half-filled shells correspond to a maximum spin state, which, due to exchange interaction, has relatively low energy. These atom-like features persist as long as $\hbar\omega_0$ is comparable to, or larger than, the interaction energy.

Fig. 3b shows the addition energy as a function of N obtained from the data shown in Fig. 1b. The spacing between the Nth and $(N + 1)$th current peaks reflects the energy to add one more electron to a dot containing N electrons. For example, the energy to add the third electron to an $N = 2$ dot can be derived from the spacing between the second and third peak. For each value of N a factor to convert gate voltage to addition energy can be determined from the Coulomb diamonds in Fig. 2. The addition energy generally becomes larger as N decreases and has large maxima for $N = 2$, 6 and 12, and also relatively large maxima for $N = 4$, 9 and 16. This N-dependence of the addition energy is consistent with the HF calculation in Fig. 3a and reflects the complete filling of the first, second and third shells as well as the half filling of the second, third and fourth shells with parallel spins. The inset in (b) shows schematically the occupation of the lowest three shells for $N = 9$. The actual value of the addition energy is smaller than that in the HF calculation, because $\hbar\omega_0$ derived from the experiment (see below) is smaller than that used in the calculation.

The electronic states are expected to be significantly modified by a magnetic field, B, applied parallel to the tunneling current. Fig. 4 shows the B-field dependence of the position of the current peaks. The positions of the first three peaks depend monotonously on B, whereas the other peaks oscillate back and forth a number of times. The number of "wiggles" increases with N. Close inspection of the figure reveals that the current peaks generally

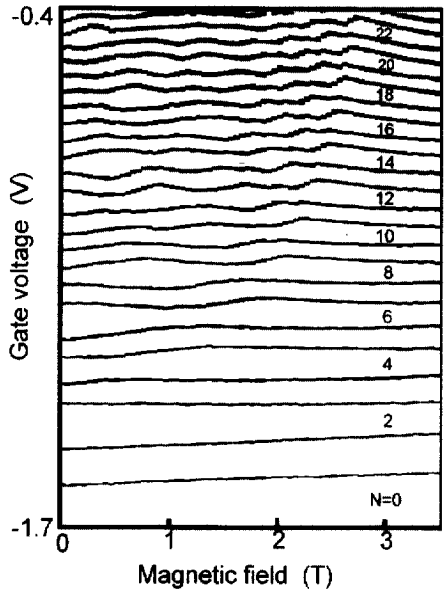

Fig. 4. Plot of the gate voltage positions of the current peaks in Fig. 1 versus magnetic field.

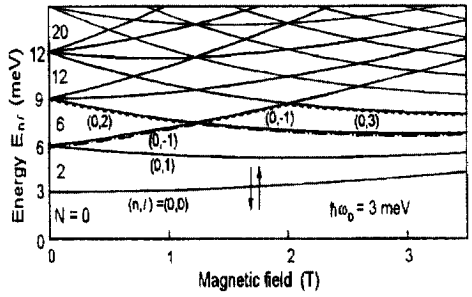

Fig. 5. Calculated single-particle energy versus magnetic field for a parabolic potential with $\hbar\omega_0 = 3$ meV. Each state is two fold spin degenerate. The dashed and dot-dashed lines are discussed in the text.

shift in pairs with B. The spacing between the peaks when N is odd is nearly constant, whereas the peak spacing varies strongly with B when N is even. This even-odd effect is particularly clear around 3.5 T, where all the peaks are evolving smoothly with B. Here the peak spacing alternates between "large" for even N and "small" for odd N. Most of these features can be explained within a single-particle framework.

If we assume a parabolic confinement, the non-interacting Schrödinger equation can be solved in the presence of a magnetic field. This calculation was first performed in 1928 and the eigenenergies are known as Darwin–Fock states [19,20]:

$$E_{n\ell} = (2n + |\ell| + 1)\hbar(\tfrac{1}{4}\omega_c^2 + \omega_0^2)^{1/2} - \tfrac{1}{2}\ell\hbar\omega_c, \qquad (2)$$

where $\hbar\omega_c = \hbar eB/m^*$ is the cyclotron energy. Fig. 5 shows E_{nl} versus B calculated for $\hbar\omega_0 = 3$ meV. Spin is neglected so each state is twofold degenerate. The degeneracies at $B = 0$ T are lifted in the presence of a B-field such that a single-particle state with a positive or negative ℓ shifts to lower or higher energy, respectively. The B-field dependence of these states gives rise to an addition energy for even N that is strongly dependent on B. On the other hand, the addition energy for odd N is determined only by the effect of Coulomb repulsion. This leads to a pairing of the conductance peaks, which is evident in Fig. 4. In Fig. 5 the energy curve for the fifth and sixth electrons (dot-dashed line) predicts that these electrons undergo a transition in their quantum numbers: (n, ℓ) changes from $(0, -1)$ to $(0, 2)$ at 1.3 T. The energy curve for the seventh and eighth electrons (dotted line) predicts that these electrons undergo transitions in (n, ℓ) from $(0, 2)$ to $(0, -1)$ at 1.3 T and then to $(0, 3)$ at 2 T. These transitions are also seen in Fig. 4. However, one should keep in mind that the charging energy separates the non-interacting states of Fig. 5 by a value which is roughly constant in magnetic field. In a similar fashion, the quantum numbers can be identified for the other electron states. Above the B-field where the last "wiggle" occurs, the single-particle states merge into the lowest spin-degenerate Landau level (i.e. for $n = 0$, $\ell \geqslant 0$). The single-particle excitation energy calculated, for example, at $B = 3.5$ T, is still large (between 1 and 1.5 meV in Fig. 5) and significantly contributes to the addition energy for even N. This leads to the alternating peak spacings observed around 3.5 T in Fig. 4 (i.e. the spacings where the even numbers have been placed are larger than the neighboring spacings).

Fig. 6a shows the B-field dependence of the third, fourth, fifth and sixth current peaks, i.e. peaks belonging to the second shell. The pairing of the third and fourth peaks, and the fifth and sixth peaks above 0.4 T is clearly seen. However, this pairing is

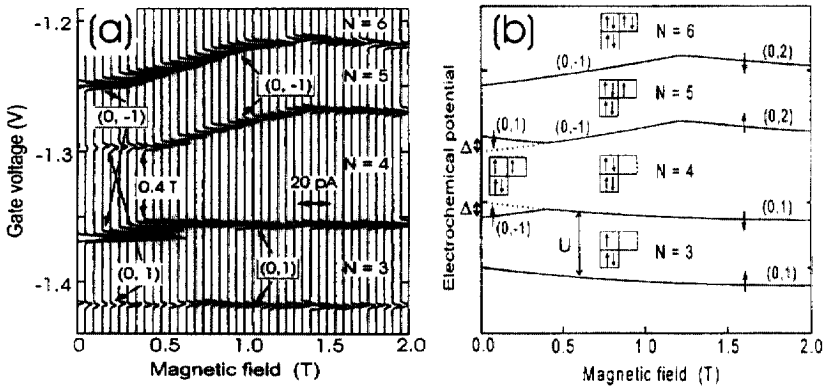

Fig. 6. (a) Evolution of the third, fourth, fifth and sixth current peaks with magnetic field from 0 to 2 T. The original data consists of current versus gate voltage traces for different magnetic fields, which are offset and rotated by 90°. (b) Calculated electrochemical potential versus magnetic field for the model described in the text and parameters $U = 3$ meV, $\Delta = 0.7$ meV, and $\hbar\omega_0 = 3$ meV. The quantum numbers (n, ℓ) are shown for the Nth electron and the diagrams show the spin configurations.

rearranged for $B < 0.4$ T. In this region the third and fifth peaks, and the fourth and sixth peaks are paired. The evolution, as a pair, of the third and fifth peak for $B < 0.4$ T is continued by the third and fourth peak for $B > 0.4$ T. Similarly, the evolution, as a pair, of the fourth and sixth peak for $B < 0.4$ T is continued by the fifth and sixth peak for $B > 0.4$ T. For $B > 0.4$ T, following the arguments related to Fig. 5, the third and fourth peaks are identified by the quantum numbers $(n, \ell) = (0, 1)$ with anti-parallel spins. The fifth and sixth peaks are identified by $(n, \ell) = (0, -1)$ with anti-parallel spins. The rearrangement of the pairing for $B < 0.4$ T can be understood in terms of *Hund's rule*, which is well known in atomic physics [21]. Hund's rule says that degenerate states in a shell are filled first with parallel spins up to the point where the shell is half filled. This is modeled in the calculation of $\mu(N)$ vs. B shown in Fig. 6b. In this figure the quantum numbers (n, ℓ) help to identify the angular momentum transitions, and the diagrams illustrate the spin configurations. In a constant interaction model, $\mu(N)$ can be written as a constant interaction energy U added to $E_{n\ell}$ [22]. To include Hund's rule in the calculation we introduce an energy Δ, which represents the energy reduction due to the exchange interaction between electrons with parallel spins. Specifically, for $N = 4$, the ground state energy is reduced if the outer two electrons have parallel spins with different angular momenta rather than anti-parallel spins with the same angular momentum. $\mu(4)$ is thus reduced by an amount Δ and there is a corresponding increase in $\mu(5)$ by Δ. This exchange effect is canceled in the presence of a B-field when the $(0, \pm 1)$ states, which are degenerate at $B = 0$ T, are split by an energy exceeding Δ. This is a simple way to include exchange effects in a constant interaction model. However, for small N we find a remarkable agreement between what is seen in Fig. 6a and that predicted in (b) with $U = 3$ meV and $\Delta = 0.7$ meV. In this model, the addition energy for $N = 4$ at $B = 0$ T is expected to be larger by 2Δ than that for $N = 3$ and 5, and this is indeed observed in Fig. 3b. This simple Hund's rule model is a first correction to the constant interaction model. A more rigorous Hartree–Fock approach, or exact diagonalization of the N-electron Hamiltonian, as outlined in Refs. [23–31], are required for a more quantitative comparison. Very recently, Eto [32] has actually been able to calculate a B-field dependence of the addition spectra that very closely duplicates the data in Fig. 4. These calculations thus confirm the simple model of Fig. 6b.

We have described that the linear transport characteristics through a 2D artificial atom reflect a shell structure, and the filling of electrons is in line with Hund's rule. The atom-like energy spectrum of the dot states is systematically modified by a magnetic field, which allows the identification of

the quantum numbers of the single-particle states. Note that the observation of orbital degeneracy implies that the system is non-chaotic, which is very unusual for solid state systems.

Acknowledgements

We would like to thank H. Akera, R.J. van der Hage, J.E. Mooij, S. Nair, Y. Tokura and H. Tamura for their help and useful discussions. L.P.K. thanks the Royal Netherlands Academy of Arts and Sciences for financial support.

References

[1] R.C. Ashoori, H.L. Störmer, J.S. Weiner, L.N. Pfeiffer, K.W. Baldwin, K.W. West, Phys. Rev. Lett. 68 (1992) 3088; R.C. Ashoori, H.L. Störmer, J.S. Weiner, L.N. Pfeiffer, S.J. Pearton, K.W. Baldwin, K.W. West, Phys. Rev. Lett. 71 (1993) 613.
[2] C.J.B. Ford, M. Field, P.J. Simpson, M. Pepper, D. Popovie, D. Kern, J.E. Frost, D.A. Ritchie, G.A.C. Jones, Inst. Phys. Conf. Ser. 127 (1992) 235.
[3] T. Fujisawa, T. Bever, Y. Hirayama, S. Tarucha, J. Vac. Sci. Technol. B 12 (6) (1994) 3755.
[4] S. Tarucha, D.G. Austing, T. Honda. Superlattices and Microstructures 18 (1995) 121.
[5] S. Tarucha, D.G. Austing, T. Honda, R.J. van der Hage, L.P. Kouwenhoven, Phys. Rev. Lett. 77 (1996) 3613.
[6] S. Tarucha, Y. Tokura, Y. Hirayama, Phys. Rev. B 44 (1991) 13815.
[7] Bo Su, V.J. Goldman, J.E. Cunningham, Science 255 (1992) 313.
[8] M. Tewordt, L. Martin-Moreno, J.T. Nicholls, M. Pepper, M.J. Kelly, V.J. Law, D.A. Ritchie, J.E.F. Frost, G.A.C. Jones, Phys. Rev. B 45 (1992) 14407.
[9] S. Tarucha, T. Honda, T. Saku, Y. Tokura, Surf. Sci. 305 (1994) 547.
[10] T. Schmidt, M. Tewordt, R.H. Blick, R.J. Haug, D. Pfannkuche, K. von Klitzing, A. Foerster, H. Lueth, Phys. Rev. B 51 (1995) 5570.
[11] J.W. Sleight, E.S. Hornbeck, M.R. Deshpande, R.G. Wheeler, M.A. Reed, R.C. Bowen, W.R. Frensley, J.N. Randall, R.J. Matyi, Phys. Rev. B 53 (1996) 15727.
[12] M.W. Dellow, P.H. Beton, M. Henini, P.C. Main, L. Eaves, Electron. Lett. 27 (1991) 134.
[13] P. Gueret, N. Blanc, R. Germann, H. Rothuizen, Phys. Rev. Lett. 68 (1992) 1896.
[14] C.J. Goodings, J.R.A. Cleaver, H. Ahmed, Electron. Lett. 28 (1992) 1535.
[15] D.G. Austing, T. Honda, S. Tarucha, Semiconductor Sci. Technol. 11 (1996) 388.
[16] V.R. Kolagunta, D.B. Janes, G.L. Chen, K.J. Webb, M.R. Melloch, Superlattices and Microstructures 17 (1995) 339.
[17] M. Macucci, K. Hess, G.J. Iafrate, J. Appl. Phys. 77 (1995) 3267.
[18] H. Tamura, private communications.
[19] V. Fock, Z. Phys. 47 (1928) 446.
[20] C.G. Darwin, Proc. Cambridge Phil. Soc. 27 (1930) 86.
[21] L.I. Schiff, Quantum Mechanics, McGraw-Hill, New York, 1949.
[22] L.P. Kouwenhoven, N.C. van der Vaart, A.T. Johnson, W. Kool, C.J.P.M. Harmans, J.G. Williamson, A.A.M. Staring, C.T. Foxon, Z. Phys. B 85 (1991) 367.
[23] L. Wang, J.K. Zhang, A.R. Bishop, Phys. Rev. Lett. 73 (1994) 585.
[24] U. Merkt, J. Huser, M. Wagner, Phys. Rev. B 43 (1991) 7320.
[25] D. Pfannkuche, R.R. Gerhardts, P.A. Maksym, V. Gudmundsson, Physica B 189 (1993) 6.
[26] G.W. Bryant, Phys. Rev. Lett. 59 (1987) 1140.
[27] C. de, C. Chamon, X.G. Wen, Phys. Rev. B 49 (1994) 8227.
[28] J.J. Palacios, L. Martin-Moreno, G. Chiappe, E. Louis, C. Tejedor, Phys. Rev. Lett. 50 (1994) 5760.
[29] Y. Tanaka, H. Akera, Phys. Rev. B 53 (1996) 3901.
[30] P.A. Maksym, T. Chakraborty, Phys. Rev. B 45 (1992) 180.
[31] P.A. Maksym, T. Chakraborty, Phys. Rev. Lett. B 65 (1990) 108.
[32] M. Eto, Jpn. J. Appl. Phys. 36 (1997) 3924.